agronomy

MDPI

Article

Fusarium Wilt of Banana Latency and Onset Detection Based on Visible/Near Infrared Spectral Technology

Cuiling Li [1,2], Dandan Xiang [3], Shuo Yang [1,2], Xiu Wang [2,4] and Chunyu Li [3,*]

[1] Information Technology Research Center, Beijing Academy of Agriculture and Forestry Sciences, Beijing 100097, China; licl@nercita.org.cn (C.L.); yangs@nercita.org.cn (S.Y.)
[2] Intelligent Equipment Research Center, Beijing Academy of Agriculture and Forestry Sciences, Beijing 100097, China; wangx@nercita.org.cn
[3] Institute of Fruit Tree Research, Guangdong Academy of Agricultural Sciences, Guangzhou 510640, China; xiangdandan@gdaas.cn
[4] National Engineering Research Center of Intelligent Equipment for Agriculture, Beijing 100097, China
* Correspondence: lichunyu@gdaas.cn

Abstract: Fusarium wilt of banana is a soil-borne vascular disease caused by *Fusarium oxysporum* f. sp. *cubense*. The rapid and accurate detection of this disease is of great significance to controlling its spread. The research objective was to explore rapid banana Fusarium wilt latency and onset detection methods and establish a disease severity grading model. Visible/near-infrared spectroscopy analysis combined with machine learning methods were used for the rapid in vivo detection of banana Fusarium wilt. A portable visible/near-infrared spectrum acquisition system was constructed to collect the spectra data of banana Fusarium wilt leaves representing five different disease grades, totaling 106 leaf samples which were randomly divided into a training set with 80 samples and a test set with 26 samples. Different data preprocessing methods were utilized, and Fisher discriminant analysis (FDA), an extreme learning machine (ELM), and a one-dimensional convolutional neural network (1D-CNN) were used to establish the classification models of the disease grades. The classification accuracies of the FDA, ELM, and 1D-CNN models reached 0.891, 0.989, and 0.904, respectively. The results showed that the proposed visible/near infrared spectroscopy detection method could realize the detection of the incubation period of banana Fusarium wilt and the classification of the disease severity and could be a favorable tool for the field diagnosis of banana Fusarium wilt.

Keywords: banana Fusarium wilt; visible/near-infrared spectroscopy; disease grading; 1D-CNN

Citation: Li, C.; Xiang, D.; Yang, S.; Wang, X.; Li, C. Fusarium Wilt of Banana Latency and Onset Detection Based on Visible/Near Infrared Spectral Technology. *Agronomy* **2024**, *14*, 2994. https://doi.org/10.3390/agronomy14122994

Academic Editors: Gerardo Fernández Barbero and Marco Scortichini

Received: 24 September 2024
Revised: 21 November 2024
Accepted: 2 December 2024
Published: 16 December 2024

1. Introduction

As an important global food crop and trade agricultural product, banana (*Musa nana* Lour.) plays an important role in social and economic development [1–3]. Banana diseases and pests are the main constraints on banana production, causing banana yield and quality losses and even regional and global fluctuations in the banana industry [4,5]. In recent years, owing to the global COVID-19 pandemic, the costs of land, labor, equipment investment, and agricultural materials for banana planting have risen, and uncertainties such as catastrophic weather have increased. Therefore, the risk of banana planting is high. A lack of banana plantation disease prevention and control measures may lead to the premature onset and aggravation of banana disease, resulting in greater losses.

At present, the world banana industry is facing a serious threat posed by the soilborne vascular fungal disease *Fusarium oxysporum* f. sp. *cubense* (Foc) [6], which is also known as yellow leaf disease or Panama disease [7,8]. The tropical race 4 strain infects almost all banana varieties. When banana plants are infected with Fusarium wilt, the pathogen releases hormones, enzymes, toxins, and other substances within the plant body, leading to certain damage to the plant and disrupting its physiological and biochemical processes; in particular, the absorption, assimilation, and transport of nutrients from the underground

to aboveground parts are seriously affected [9]. The nutrient contents of nitrogen (N), available phosphorus (P), and available potassium (K), which are essential for plant growth, are notably reduced. The reduction in nutrient elements, especially nitrogen, leads to the reduction in chlorophyll cell formation, chlorophyll content, and green leaf area index, and the photosynthetic ability of banana leaves is weakened. Banana leaves gradually turn yellow from bottom to top until they wilt, and the vascular bundles of the root will gradually turn red-brown and eventually turn dark black.

Banana Fusarium wilt is a devastating disease faced by the banana industry worldwide; generally, the yield is reduced by more than 20%, and in severe cases, banana plantations may even have no harvest. Due to its long incubation period and high infectivity, banana Fusarium wilt has a large impact range and is difficult to detect in advance [10]. Once a diseased plant is identified, the diseased plant should be uprooted quickly, lime should be applied to the affected area, and the diseased plant should be removed from the banana plantation and treated with lime for deep burial or for drying and then burning. At present, there is still a lack of suitable disease-resistant banana varieties in production, and there is no method that can completely cure banana Fusarium wilt [11]. Banana plantations infected with Fusarium wilt need to be evaluated for their infection degree so that fruit farmers can make the best decision on when to stop planting in this area. Therefore, it is particularly important to use rapid and accurate banana Fusarium wilt detection technology for quickly identifying the latent disease and determining the disease severity during the onset period, allowing for timely destruction and isolation measures to control the spread of the disease [12,13].

Conventional methods for banana Fusarium wilt detection mainly include artificial morphological identification, physiological and biochemical identification, and molecular biological identification. Molecular biological identification includes (polymerase chain reaction) PCR [14,15], real-time fluorescence PCR [16], and loop-mediated isothermal amplification approaches [17–19]. Artificial morphological identification cannot identify asymptomatic latent diseases, is easily confused with other diseases, and has subjective dependence and low efficiency. Physiological and biochemical identification and molecular biological identification usually have high detection accuracy, but the detection process is complex, laborious, time-consuming, inefficient, and destructive to the sample [20] and thus cannot meet the needs of rapid modern agriculture development. Visible/near-infrared spectroscopy has the characteristics of reflecting the internal structure and component information of objects. When plants are infected, the water content, pigment content, and internal structure of the leaves change, and these changes are reflected in the spectral characteristics [21]. The application of visible/near-infrared spectroscopy technology in the detection of banana Fusarium wilt has the advantages of fast detection speed, high analysis efficiency, and nondestructive sampling. At present, the research on the rapid and nondestructive detection of banana Fusarium wilt by domestic and foreign scholars is still relatively limited, and there is no research on the rapid nondestructive detection of the banana Fusarium wilt incubation period using visible/near-infrared spectroscopy. Shimin Zhang et al. [12]. established an optimal canopy classification model of different infection stages according to the canopy spectral characteristics of banana plants infected with Fusarium wilt. Through a comprehensive evaluation of the classification results of different supervised and unsupervised modelling methods, the authors suggested using the unsupervised hotspot analysis (HA) method for banana Fusarium wilt identification, especially in the late infection stage, and the random forest (RF) monitoring method was recommended for early infection to achieve slightly higher accuracy. Gloria Valentine Nakato et al. [22] established an agricultural network between fruit farmers and scientists through mobile phones for monitoring banana diseases in Uganda and monitored three banana diseases in Uganda based on plant photos, as follows: banana Xanthomonas wilt (BXW), Fusarium wilt (FW), and banana bundt top disease (BBTD). Yi-Jia Lin et al. [13]. constructed the Raman spectral fingerprint of banana pseudostem samples with different degrees of disease in Taiwan, and the Fusarium wilt of banana (FWB) detection rate in asymptomatic banana

samples was 76.2% using the Raman spectral method. Huichun Ye et al. [23]. evaluated the performance of supervised classification algorithms, i.e., support vector machine (SVM), random forest (RF), and artificial neural network (ANN), in identifying and positioning the occurrence and nonoccurrence of banana Fusarium wilt based on unmanned aerial vehicle (UAV) multispectral images. The results showed that the SVM, RF, and ANN algorithms achieved good performance in recognizing and mapping banana Fusarium wilt based on UAV multispectral images. The above research studies used UAV-based multispectral imagery, Raman spectroscopic fingerprints, and plant imaging methods to detect banana Fusarium wilt, but these methods either had low accuracy in detecting the latent period of banana Fusarium wilt, or cannot detect the latent period of banana Fusarium wilt. The visible/near-infrared spectroscopy detection technology used in this study had advantages in detecting the latent period of banana Fusarium wilt and had a high detection accuracy.

The spectral data collected by a visible/near-infrared spectrometer contain not only the self-information of the sample but also other irrelevant information and noise, such as electrical noise, sample background and stray light [24,25]. Therefore, when building models with machine learning methods, preprocessing methods aimed at eliminating irrelevant information and spectral noise become critical and necessary. Different preprocessing methods have different effects on the built model [26]. Since a single preprocessing method can only suppress a certain type of interference, a combination of different preprocessing methods is usually used to remove various types of spectral interference [27,28]. Supervised learning method is a type of machine learning method that is currently widely studied. For example, K-nearest neighbors [29], decision trees [30], backpropagation (BP) neural networks [31], and extreme learning machines [32] have been successfully applied in plant disease and pest detection. These classifiers can learn the features of the target class from the training samples and apply this information to the unclassified data.

The research objective was to develop a rapid method to grade and detect banana Fusarium wilt latency and the onset period based on visible/near-infrared spectroscopy technology, establish a disease severity classification model using supervised learning algorithms, and determine the optimal disease grade classification method, providing technical and methodological support for the early control of banana Fusarium wilt.

2. Materials and Methods

2.1. Visible/Near-Infrared Spectrum Acquisition System

The visible/near-infrared spectrum acquisition system used in this study consisted of a portable detection mainframe (HL 10000-Mini, Shanghai Ruihai Optoelectronic Technology Co., Ltd., Shanghai, China), a handheld probe (QP600-1-VIS-NIR, Shanghai Ruihai Optoelectronic Technology Co., Ltd., Shanghai, China), and a data processor (ThinkPad X260, Lenovo Group Co., Ltd., Beijing, China), and its schematic diagram is shown in Figure 1. The internal structure of the portable detection mainframe, as shown in Figure 2, mainly consisted of a visible/near-infrared spectrometer, a halogen light source, a reference whiteboard, an optical fiber, and a computer to realize the spectral data acquisition of banana leaves. The visible/near-infrared spectrometer was a miniature spectrometer (Uspectral-RIT-2.7.0, Shanghai Fuxiang Optics, Shanghai, China) with a spectral range of 336~1078 nm and a spectral resolution of 0.36 nm. The spectral data of banana leaves were collected using the external trigger mode. The halogen light source (HL-10,000 min) provided stable illumination for the portable detection mainframe. The working voltage of the portable detection mainframe was DC (12 V). The reference whiteboard was used to calibrate the spectral data, the data interface was connected to the portable detection mainframe and the data processor, the trigger interface was connected to the portable detection mainframe and the handheld probe, the probe interface was connected to the portable detection mainframe and the handheld probe, and a strap was used for the user to carry the portable detection mainframe. The handheld probe contained an optical fiber, a handle, a trigger button, and a trigger line. The user brought the handheld probe into contact with the target position on the banana leaf, forming a sealed chamber, and pressed the trigger

button to initiate the portable detection mainframe, allowing the collection of spectral data. The fiber was a Y-type fiber, the fiber probe end and the handle were connected to form a single unit, the light inlet port end was connected to the light source, and the light outlet end was connected to the spectrometer. The trigger button was connected to the trigger line, and the user operated the trigger button to send a signal to the portable detection mainframe. The data processor was mainly a computer or an embedded device that was used to read, process, and save spectral data, establish mathematical models, and obtain the banana Fusarium wilt detection results.

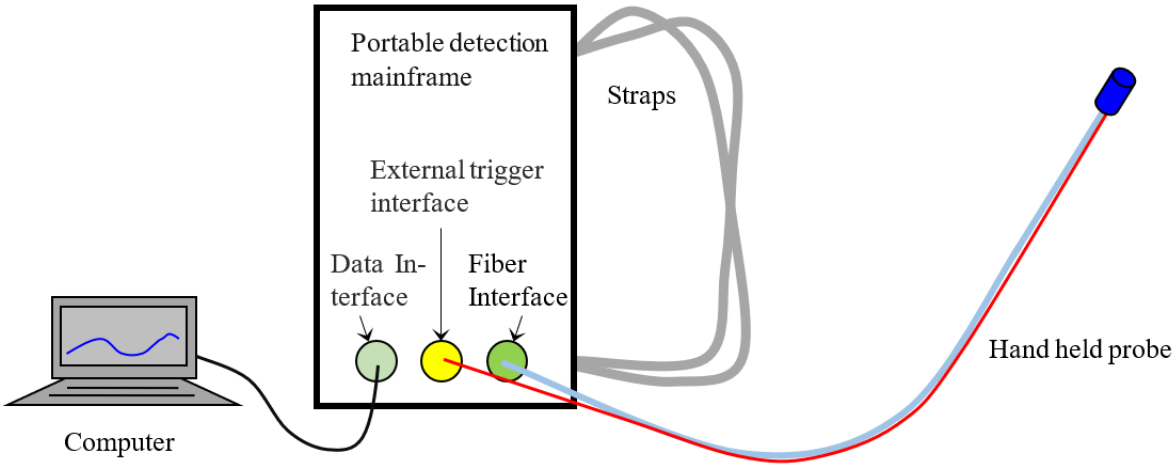

Figure 1. Structure schematic diagram of the visible/near-infrared spectrum acquisition system.

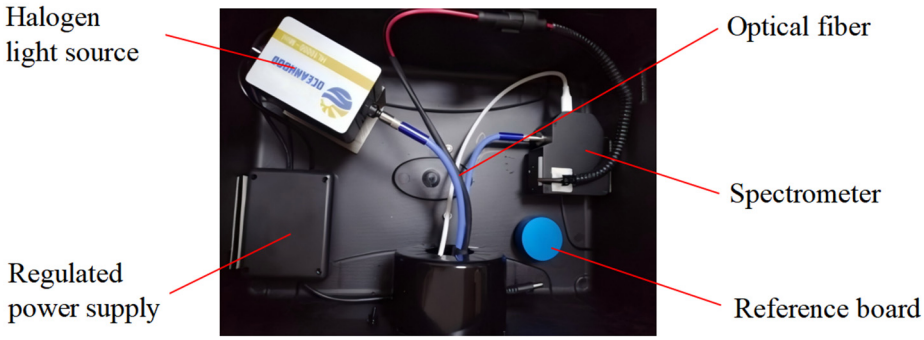

Figure 2. Internal structure diagram of the portable mainframe.

2.2. Sample Preparation

Banana leaf samples were selected in September 2020, from the banana planting demonstration base of the Fruit Tree Research Institute of the Guangdong Academy of Agricultural Sciences in China by specialized technicians with rich experience in banana plantation management and disease identification during the high incidence period of the disease. The banana variety was *Musa brasiliensis*. In this study, according to the classification standard of banana Fusarium wilt [33], the banana leaves were divided into the following grades: "Grade 0" for healthy leaves; "Grade 1" for asymptomatic, disease latent leaves; "Grade 2" for leaves with small yellow patches covering less than 25% of the total leaf area; "Grade 3" for leaves with large yellow patches covering 26–50% of the leaf area; and "Grade 4" for leaves with large yellow patches covering 51% to 75% of the total leaf area. In this study, there were 24 "Grade 0" leaf samples, 21 "Grade 1" leaf samples, 22 "Grade 2" leaf samples, 22 "Grade 3" leaf samples, and 17 "Grade 4" leaf samples, totaling 106 leaf samples. Each banana leaf sample from "Grade 0" to "Grade 4" was numbered in order. Leaf samples of each grade were randomly selected during numbering. Samples numbered as 4 or multiples of 4 were selected as test set samples,

totaling 26 samples, and the remaining 80 samples were used as training set samples. Table 1 shows the sample numbers of the training set and the test set for each disease grade.

Table 1. Numbers of the training set and the test set of samples for each disease grade.

	"Grade 0"	"Grade 1"	"Grade 2"	"Grade 3"	"Grade 4"
Training set	18	16	17	16	13
Test set	6	5	5	6	4
Total number	24	21	22	22	17

2.3. Spectral Data Acquisition and Preprocessing

2.3.1. Spectral Data Acquisition

To acquire spectral data, the portable detection mainframe was connected, the handheld probe and the data processor were turned on correctly, the power and light source were turned on, and the detection mainframe was preheated for 15 min to ensure that the light source and spectrometer were in a stable working state. Next, the spectral information of the standard reference whiteboard was collected. Then, the light path was cut off, and the spectral information of the dark environment was collected. The spectrometer automatically performed white reference calibration and black reference calibration on the subsequently collected reflectance spectral data of banana leaf samples, and the reflectance spectral data were saved automatically. There were 106 sets of original reflectance spectral data of leaf samples collected on the spectral data acquisition site as shown in Figure 3, and the original reflectance spectral data of 106 banana leaves are shown in Figure 4. The bands with large noise signals at both ends were removed. The effective wavelength range was 450–900 nm. The average reflectance spectra of banana leaves in the same disease grade were calculated, and the curves of the average reflectance spectra of banana leaves for the five disease grades are shown in Figure 5. In this figure, as the disease grade increased, the spectral reflectance also increased in the wavelength range of 500~700 nm.

Figure 3. Spectral data acquisition and the red dot on the left image represents the site where the symptom was observed and the spectral data were taken.

2.3.2. Data Augmentation

Due to the large number of parameters in a convolutional neural network model, a large amount of labeled sample data is required to train the model. Therefore, in this study, the method of patent [34] was followed to perform augmentation on the 106 sets of raw reflectance spectra data. The method of light simulation was used to simulate the original spectral data, and expanded the spectral data by adding a series of light disturbances within a certain range, effectively increasing the number of spectral data. After data augmentation, a total of 1060 sets of spectral data containing disease information of samples with different disease grades were obtained.

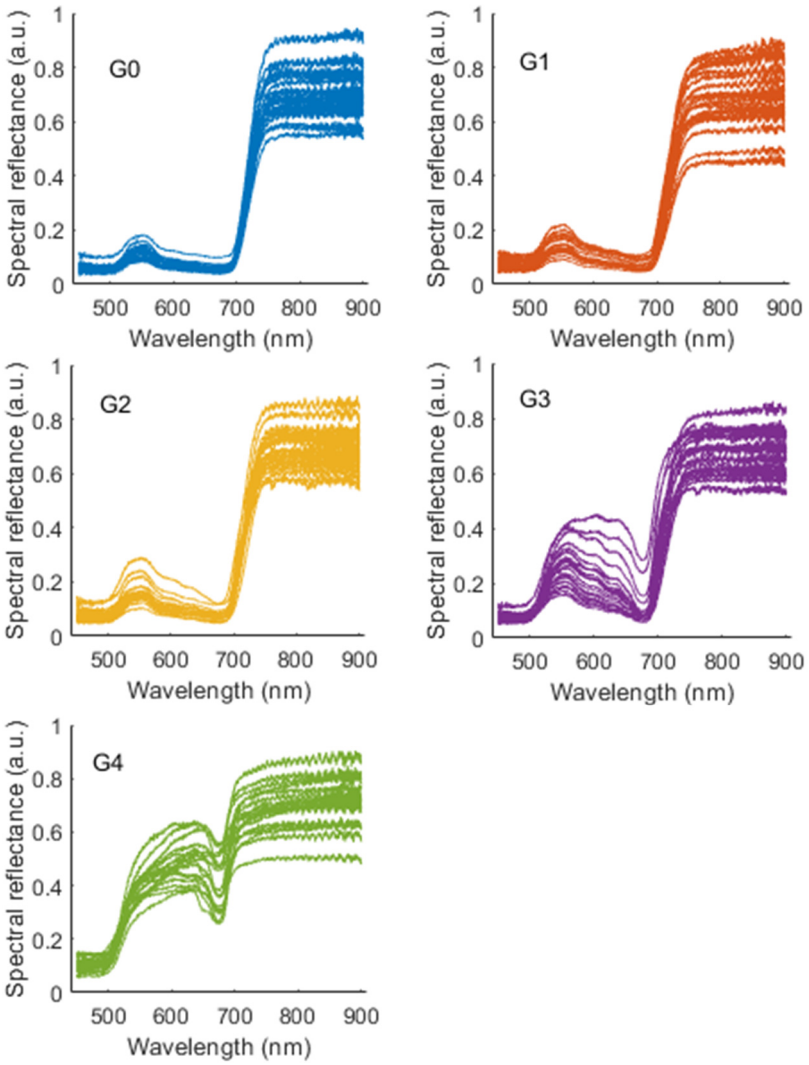

Figure 4. Original reflectance spectrum of banana leaf samples. G0, G1, G2, G3, and G4 represent disease "Grade 0", "Grade 1", "Grade 2", "Grade 3", and "Grade 4", respectively.

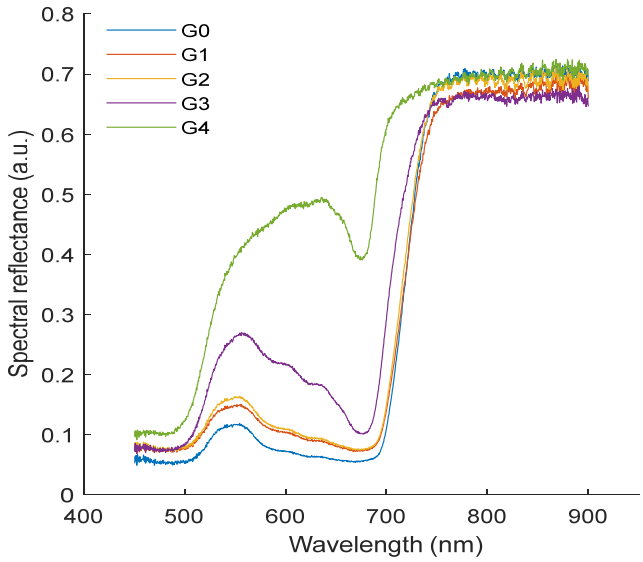

Figure 5. Average original reflectance spectral curves of banana leaves for the five disease grades.

2.3.3. Preprocessing of Spectral Data

In the process of visible/near-infrared spectroscopy data acquisition, due to the influence of the sample background, morphological differences, and measurement conditions, spectral data are prone to containing random noise. Therefore, spectral data preprocessing is of great significance. Effective preprocessing methods can reduce or even eliminate spectral noise, improve the spectral signal-to-noise ratio, improve the modelling efficiency and the model prediction accuracy, and enhance the model generalization and stability. Spectral data preprocessing methods are mainly divided into baseline correction, scatter correction, smoothing, signal enhancement, and noise cancellation. The first derivative (FD) processing of spectral data can effectively eliminate the baseline drift and other background interference, distinguish overlapping peaks, and improve the resolution and sensitivity. However, the FD preprocessing method will amplify the noise, so it is necessary to smooth the original spectral data. The Savitzky-Golay (SG) convolution smoothing method is a widely used denoising method that can effectively eliminate the fine white noise of spectral data. Multiplicative scatter correction (MSC) is mainly used to eliminate the influence of the nonuniform distribution of solid particles and the variation in particle size, surface scattering, and optical path on diffuse reflectance spectra. In this study, the FD, MSC, and SG convolutional smoothing methods and various combinations of these methods were used to preprocess the spectral data.

2.4. Principal Component Analysis of Spectral Data

Although the effects of spectral noise, baseline drift, and stray light were eliminated after the original spectra of the banana leaves were preprocessed by FD, MSC, and SG convolution smoothing, there were 1201 variables in the 450–900 nm spectrum range. In addition, there was still a certain correlation between the variables that increased the complexity of data analysis to a certain extent and affected the classification effect of the model. Feature extraction can be used to reduce the dimension of the spectral data, reduce the redundancy of the data, optimize the effective spectral information, and improve the classification accuracies of the models. In this study, principal component analysis (PCA) was used to extract features from the spectral data of the banana leaves to reduce the redundancy and correlation of the spectral data. The principal components were extracted by calculating the eigenvalues and eigenvectors of the covariance matrix [35]. Principal component analysis recombines the original variables with certain correlations into a new set of independent comprehensive variables to replace the original variables. Under the premise of losing a minimal amount of information, the multiple variables are transformed into several comprehensive variables. Each principal component is a linear combination of the original variables, and each principal component is uncorrelated with other principal components, leading to the superior performance with the principal components over that with the original variables [36].

2.5. Modelling Method of Disease Severity Classification

2.5.1. Fisher Discriminant Analysis

Fisher discriminant analysis (FDA) projects high-dimensional pattern samples into the optimal discriminant vector space to extract classification information and reduce the dimension of the feature space. After projection, the pattern samples in the new vector space exhibit the minimum intraclass distances and the maximum interclass distances. In this study, the FDA function was established according to the principle of the maximum discrete distance between classes and the minimum discrete distance within classes. Then, the discrimination analysis of the tested samples was carried out according to the FDA function. The principal components of a banana leaf sample are $PC^n = \left(pc_1^n, pc_2^n, \ldots, pc_m^n\right)^{\mathrm{T}}$ after preprocessing and PCA dimension reduction. The projection formula is as shown in Equation (1).

$$f\left(PC^n\right) = \sum_{i=1}^{m} c_i pc_i^n + c_0 \quad (1)$$

where $f\ (PC^n)$ is the projection function; n = 1, 2, 3, . . . , 106, m is the number of principal components; pc_i^n is a one-dimensional variable; c_i is the projection coefficient of the variable pc_i^n; and c_0 is a constant term.

2.5.2. Extreme Learning Machine Classification

The ELM is a single hidden layer feedforward neural network learning method proposed by Huang [37], and its structure is similar to that of the BP neural network and other traditional neural networks. In the ELM learning process, the weights from the input layer to the hidden layer and the threshold of the hidden layer can be randomly initialized, and the weights from the hidden layer to the output layer are obtained by solving the matrix equation. The ELM does not require complex calculations and can quickly complete network learning [38]. Due to its high learning efficiency, high accuracy, and strong generalizability, the model is widely used in the field of data classification and pattern recognition. The ELM consists of an input layer, a hidden layer, and an output layer. The input layer has n neurons corresponding to n input variables, the hidden layer has l neurons, and the output layer has m neurons corresponding to m output variables.

Suppose the input matrix of the training set with D samples is X and the output matrix is Y, the connection weights between the input layer and output layer are ω, the connection weights between the hidden layer and output layer are β, the threshold of the hidden layer neurons is b, the activation function of the hidden layer neurons is $g(x)$, and the output of the neural network is T. The goal of single-hidden layer neural network learning is to minimize the training error of the output, which can approach an arbitrary $\varepsilon > 0$, as shown in Equation (2), that is, there exist ω, β, and b:

$$\sum_{j=1}^{D} \|Y - X\| < \gamma \tag{2}$$

In the classification process, once ω and b are randomly determined, the connection weights β between the hidden layer and the output layer are uniquely determined. The mathematical model of the extreme learning machine can be obtained as shown in Equation (3):

$$\mathrm{elm}(X) = \|T - X\| \tag{3}$$

2.5.3. One-Dimensional CNN

CNN is a type of feedforward neural network that includes convolutional computation and has deep structure, and is one of the representative algorithms of deep learning [39]. One dimensional convolutional neural network (1D-CNN) is a variant of convolutional neural network used for processing sequential data [40,41]. Compared with traditional fully connected neural networks, 1D-CNN can effectively utilize local patterns in the data, resulting in better performance in processing sequential data.

The 1D-CNN consists of an input layer, several convolutional layers, several pooling layers, several fully connected layers, and an output layer. It typically consists of multiple alternating convolutional and pooling layers, and finally uses fully connected layers to map the extracted features to the output. During the training process, 1D-CNN uses a backpropagation algorithm to update model parameters to minimize the loss value. Among them, convolutional layers are used to extract local features, pooling layers are used to reduce the dimensionality of features, and fully connected layers are used for classification or regression tasks. When using 1D-CNN, we usually need to set some hyperparameters, such as the size of the convolutional kernel, the number of convolutional layers, and the pooling operation method. The selection of these hyperparameters will affect the performance and efficiency of the model.

The network structure of the 1D-CNN constructed in this study is shown in Figure 6, which consists of one input layer, three convolutional layers, three activation layers, three pooling layers, one fully connected layer, and one output layer. The cross-entropy loss

function was used as the index of model updating, and Adam was used as the model optimizer. After determining the network structure, it was necessary to optimize the hyperparameters of the 1D-CNN model, among which the learning rate is the most important hyperparameter, which can accelerate model convergence and avoid falling into local optima. Therefore, optimizing the learning rate was chosen in this study. The learning rates were set to 0.01, 0.005, 0.001, 0.0005, 0.0001, and 0.00005, respectively, and compared the convergences and accuracies of the models under different learning rates by analyzing the loss values and accuracies of the training and test sets, and ultimately the optimal learning rate was selected.

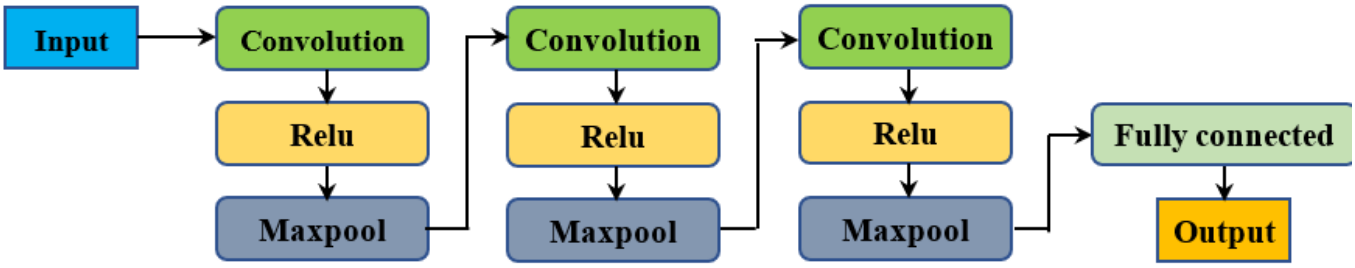

Figure 6. The 1D-CNN network structure of the banana Fusarium wilt disease grading model.

3. Results and Discussion

3.1. Results

3.1.1. Results of Preprocessing of Spectral Data

In this study, the FD, MSC, and SG preprocessing methods and combinations of more than two preprocessing methods were used to preprocess the original spectral data. The derivative order of the SG smoothing method was '0', the polynomial degree was '5', and the number of smoothing points was '25'. The step size of FD was '1'. Figure 7 shows the spectral curves of the reflectance spectral data of the banana leaf samples after SG smoothing preprocessing. The spectral curves of leaves with disease Grades 0, 1, and 2 are close, and the spectra of the other grades are quite different.

3.1.2. Results of Principal Component Analysis

In this study, the wavelength range of the effective spectrum was 450–900 nm, which included 1201 variables. PCA was used to extract the principal components and reduce the dimension of the spectral data, the contribution rates of the principal components were sorted from largest to smallest, and the principal components with a cumulative contribution rate of 85% were selected to determine the number of principal components and their respective scores. PCA was carried out on the original spectral data, and two principal components were extracted. The eigenvalue of the first principal component was 739.35, with a contribution rate of 61.56%, the eigenvalue of the second principal component was 371.97, with a contribution rate of 30.97%, the eigenvalue of the third principal component was 60.43, with a contribution rate of 5.03%, and the cumulative contribution rate of the two principal components was 92.53, effectively reflecting the information of the original spectral data. The score coefficient curve of the first principal component is shown in Figure 8, and the three-dimensional space was constructed by PC1, PC2, and PC3, the disease grade distribution of 106 samples in the three-dimensional space is shown in Figure 9. The score coefficient of this principal component could effectively reflect the contribution of various original variables to this component. As shown in the figure, the green light waveband at 525 nm and the red edge waveband at 725 nm, which are closely related to plant disease and pest information, were important in reflecting the first principal component. Therefore, the wavebands at 525 nm and 725 nm are sensitive wavebands for banana Fusarium wilt. When the spectral data were preprocessed by SG-FD-MSC for principal component analysis, a total of 29 principal components were extracted.

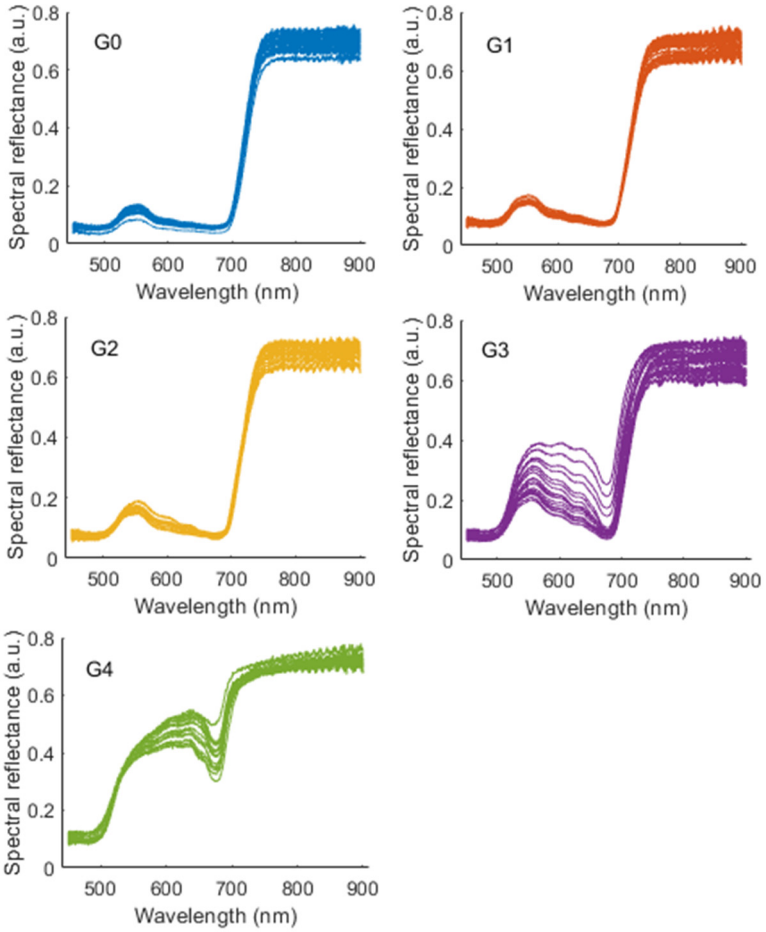

Figure 7. Reflectance spectra curves after pretreatment with SG smoothing method.

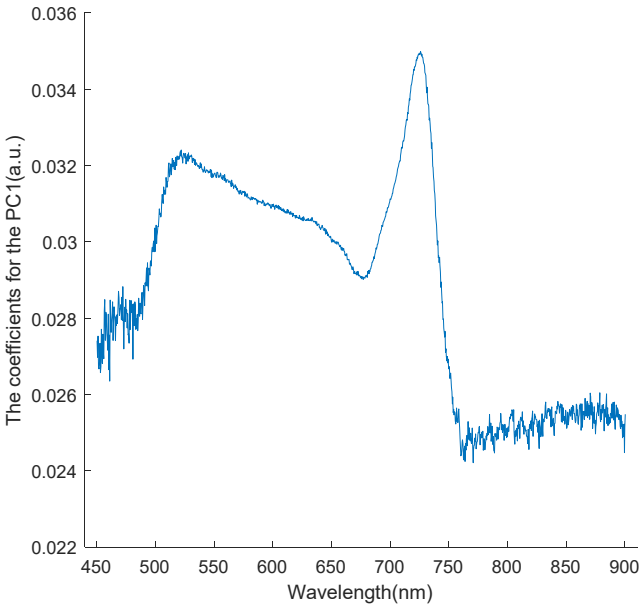

Figure 8. Score coefficient curves of the first principal component PC1 based on the original spectral data.

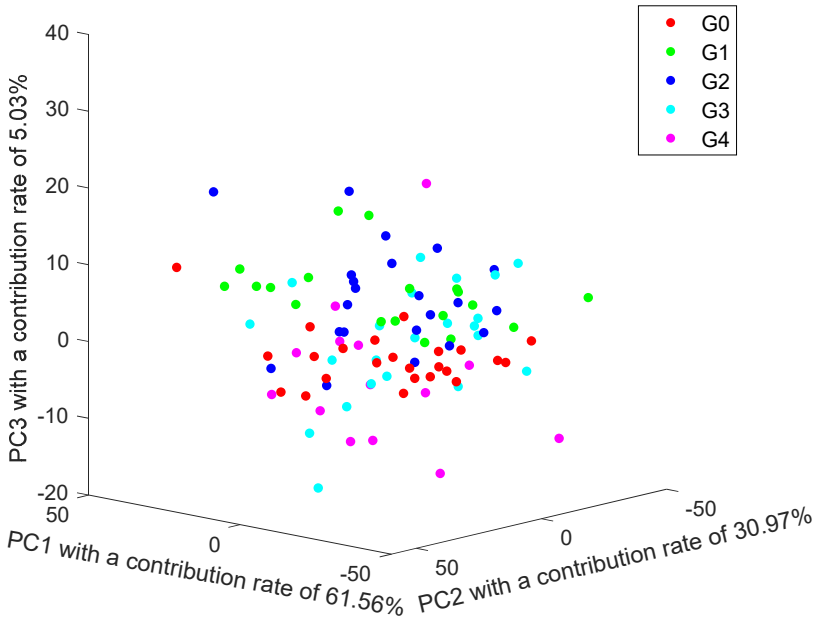

Figure 9. The 3D distribution of PC1, PC2, and PC3 based on the original spectral data.

3.1.3. Results of Banana Fusarium Wilt Disease Severity Classification

Based on the SG, FD, and MSC preprocessing methods and combinations of more than two preprocessing methods, the principal components extracted by PCA, FDA, ELM, and 1D-CNN were used to establish banana Fusarium wilt disease severity classification models.

FDA Classification Results of Banana Fusarium Wilt Disease Severity

FDA based on principal components was performed to establish a banana leaf Fusarium wilt disease grade classification, and the classification effects of the model are shown in Table 2. The FDA classification model based on FD-MSC-SG preprocessing method had the best modeling effect, and the classification accuracy (ACC) on the test set samples was 0.891, the precision (PREC) was 0.900, the recall (REC) was 0.891, the F1 score (F1S) was 0.890, and the classification training error rate (TER) was 0.001. The FDA classification model based on FD or FD-MSC preprocessing method had a worse modeling effect than the FDA classification model developed without preprocessing method. The FD preprocessing method weakened the modeling effect, while SG and MCS improved the modeling effect. The FD preprocessing method not only eliminated baseline drift and improved the resolution of overlapping peaks, but also amplified small noise, resulting in poor model performance. The FD preprocessing method needed to be combined with other preprocessing methods that can reduce spectral noise to improve model performance, such as the FD-SG-FDA model. Thus, it can be seen that spectral data preprocessing played an important role in the FDA model, so choosing the appropriate preprocessing method was essential.

Table 2. Modeling effects of disease grade classification based on FDA.

PREM	N_{PC}	TER	PREC	REC	F1S	ACC
OD	2	0.339	0.657	0.672	0.659	0.664
FD	124	0.021	0.442	0.414	0.424	0.396
MSC	3	0.225	0.768	0.772	0.766	0.762
SG	2	0.130	0.867	0.865	0.865	0.864
FD-SG	29	0.003	0.718	0.719	0.705	0.713
MSC-SG	2	0.155	0.848	0.849	0.849	0.842
FD-MSC	116	0.020	0.287	0.284	0.262	0.294
FD-MSC-SG	29	0.001	0.900	0.891	0.890	0.891

Note: PREM stands for preprocessing method; N_{PC} denotes the number of principal components; OD means the original data.

After FD-MSC-SG preprocessing and PCA dimension reduction, 29 principal components were extracted from the reflectance spectral data. Based on the principal components, the FDA model of disease grade classification of banana Fusarium wilt was established. The classification function of the leaf sample disease grade to be classified as grade i or grade j is $F_{(i,j)}$ $(pc_1, pc_2, pc_3, \ldots, pc_{29})$, where $i \in (0, 1, 2, 3, 4)$, $j \neq i$, $j \in (0, 1, 2, 3, 4)$. The condition for sample x to be classified as grade i instead of grade j was that the classification function satisfies Equation (4); otherwise, sample x was determined as class j. The classification results of the SG-FD-MSC-FDA model on the test set samples are shown in Figure 10. The classification accuracies of banana leaf Fusarium wilt "Grade 0", "Grade 1", "Grade 2", "Grade 3", and "Grade 4" were 0.98, 0.62, 0.87, 0.98, and 1, respectively. The SG-FD-MSC-FDA model could distinguish healthy banana leaves, moderate Fusarium wild disease leaves, mild Fusarium wild disease leaves, and severe Fusarium wild disease leaves. However, the accuracy of identifying Fusarium wild incubation period leaves was low, making it easy to mistake them for healthy banana leaves.

$$coe \times x + con > 0 \tag{4}$$

where *coe* is the coefficient and *con* is the constant of the linear function.

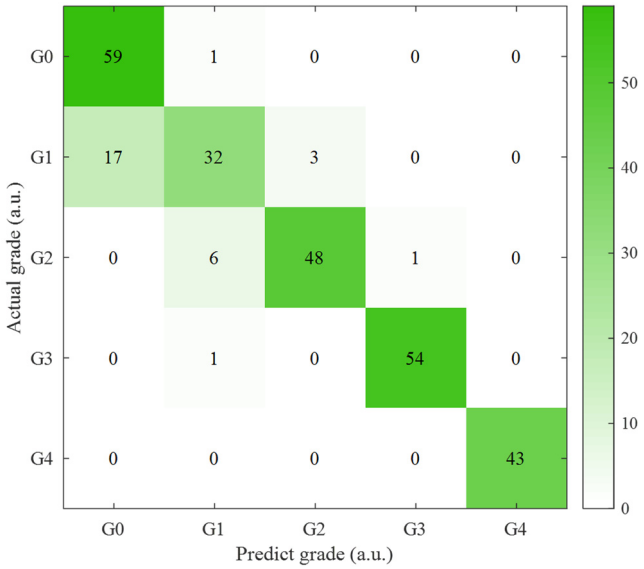

Figure 10. Disease grade classification results on test set of FD-MSC-SG-FDA model. G0, G1, G2, G3, and G4 represent disease "Grade 0", "Grade 1", "Grade 2", "Grade 3", and "Grade 4", respectively.

ELM Classification Results of Banana Fusarium Wilt Disease Severity

Based on the principal components, the ELM method was used to establish the banana leaf Fusarium wilt disease grade classification model. The classification effect of the model when the number of neurons in the hidden layer was set to 30 is shown in Table 3. When modelling was based on the MSC-SG preprocessing method, the ELM classification model had the best effect, and the classification ACC on the test set samples was 0.99, the PREC was 0.99, the REC was 0.99, the F1S was 0.99, and the NAE was 4.90. When modelling without a preprocessing method, the ELM classification model had the classification ACC on the test set samples of 0.63, the PREC of 0.64, the REC of 0.64, the F1S of 0.60, and the NAE of 14.00. The FD-ELM, FD-SG-ELM, and FD-MSC-ELM models had a worse effect than the model developed without preprocessing methods.

The FD preprocessing method weakened the model performance, while the MSC and SG preprocessing methods improved the model performance. The FD preprocessing method not only improves the resolution of overlapping peaks, but also amplifies noise signals. The goal of FDA is to find a linear projection that enables the best class separation

of the projected data points in the new space, which can reduce the impact of noise on the model to some extent. ELM does not distinguish between effective signals and noise signals for classification modeling, so the classification performances of FD-FDA, FD-SG-FDA, FD-MSC-FDA, and FD-MSC-SG-FDA models are better than those of FD-ELM, FD-SG-ELM, FD-MSC-ELM, and FD-MSC-SG-ELM models. The FD-SG-ELM model has a better classification performance, while the FD-MSC-ELM model has a poorer classification performance because the SG preprocessing method can eliminate the influence of noise.

Table 3. Modeling effects of disease grade classification based on ELM.

PREM	N_{PC}	NAE	PREC	REC	F1S	ACC
OD	2	14.000	0.642	0.641	0.602	0.634
FD	124	21.772	0.365	0.359	0.361	0.355
MSC	3	9.000	0.856	0.856	0.853	0.853
SG	2	11.489	0.823	0.808	0.811	0.804
FD-SG	29	20.445	0.480	0.482	0.477	0.475
MSC-SG	2	4.899	0.989	0.988	0.989	0.989
FD-MSC	116	34.713	0.186	0.187	0.184	0.192
FD-MSC-SG	29	14.799	0.752	0.739	0.737	0.736

After MSC-SG preprocessing and PCA data dimension reduction, a total of two principal components were eventually extracted. Based on the principal components, ELM classification models of banana Fusarium wilt disease grade were established. The number of neurons in the input layer was two, the number of neurons in the output layer was one, the activation function was the sigmoid function, and the function was continuous and smooth in the domain of definition and derivable everywhere. Let the number of neurons in the hidden layer be 5, 10, 15, …, 100. Figure 11 shows the influence of the number of neurons in the hidden layer on the performance of the ELM. As observed in this figure, more neurons in the range of 0 to 100 in the hidden layer meant that the model effect was better. When the number of neurons in the hidden layer was less than or equal to 40, the classification ACC on the training set and the test set showed a fluctuating upward trend. When the number of neurons in the hidden layer was >40 and $\leq$100, the classification accuracies on the training set and test set showed stable trends. When the number of neurons in the hidden layer was 30, the disease grade classification results of the test set are shown in Figure 12; the classification ACC of the test set of banana Fusarium wilt latency samples was 1, and the disease grade classification ACC was 0.99. One set of spectral data of healthy "Grade 0" leaf was misjudged as mildly affected "Grade 2" dataset, one set of spectral data of moderately affected "Grade 3" leaf was misclassified as incubation period-affected "Grade 1" dataset, and one set of spectral data of severely affected "Grade 4" leaf was misclassified as healthy "Grade 0" dataset.

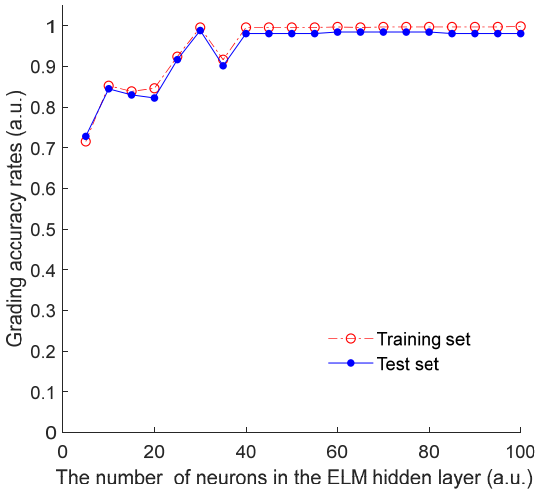

Figure 11. Influence of the number of hidden layer neurons on the MSC-SG-ELM model.

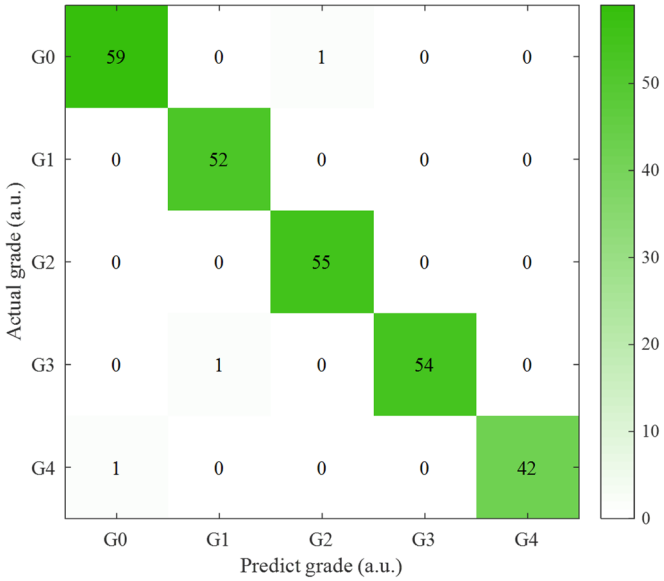

Figure 12. Disease grade classification results of MSC-SG-ELM model on test set. G0, G1, G2, G3, and G4 represent disease Grade 0, Grade 1, Grade 2, Grade 3, and Grade 4, respectively.

One-Dimensional CNN Classification Results of Banana Fusarium Wilt Disease Severity

The 1D-CNN model was constructed based on unprocessed spectral data. In the 1D-CNN network structure, the number of filters in the first convolutional layer was 64, the size of the convolution kernel was 21, and the stride was 1. The number of filters in the second convolutional layer was 64, the size of the convolution kernel was 19, and the stride was 1. The number of filters in the third convolutional layer was 64, the size of the convolution kernel was 17, and the stride was 1. The convolution kernel size of the three pooling layers was 3, and the stride was 3, using the maximum pooling method. The batch size for model training was 53, with 50 iterations. The learning rate plays a crucial role in obtaining the optimal weight values, generally speaking, a low learning rate means that it takes long time to train the model, while a high learning rate can lead to model instability. In this study, the learning rates were set to 0.01, 0.005, 0.001, 0.0005, 0.0001, and 0.00005, respectively, the effects were compared of different learning rates on the loss values and accuracies of the models, and the optimal learning rate was selected to establish the classification model of banana Fusarium wilt disease grading detection.

In CNN models, when the learning rate is high, the model cannot be trained, when the learning rate is moderate, a model with good accuracy can be trained, and when

the learning rate is low, it takes a long time to reach the same accuracy as a model with moderate learning rate. From Figures 13 and 14, it can be seen that as the number of iterations increases, the loss values of the training set and test set continue to decrease, while the accuracy continues to improve. In this study, when the learning rate values were moderate, such as 0.0001 and 0.0005, the model's loss and accuracy could quickly reach their optimal values; when the learning rate values were low, such as 0.00005, it took a longer time for the model's loss value and accuracy to reach the same level as models with moderate learning rates; as shown in Figure 15, when the learning rate values were high, such as 0.01, the loss values and accuracies of the models presented significant oscillations for a long time and gradually approached the optimal values. In this study, when the learning rate was 0.0005, the changes in the loss values and accuracies of the model's training set and test set first stabilized at 13 iterations. The model with the learning rate value of 0.0005 had the best classification performance, so the learning rate of the 1D-CNN model in this study was set to 0.0005, and the accuracy of the model test set reached to 0.904. In summary, the constructed 1D-CNN model could effectively achieve grading detection of banana Fusarium wilt disease.

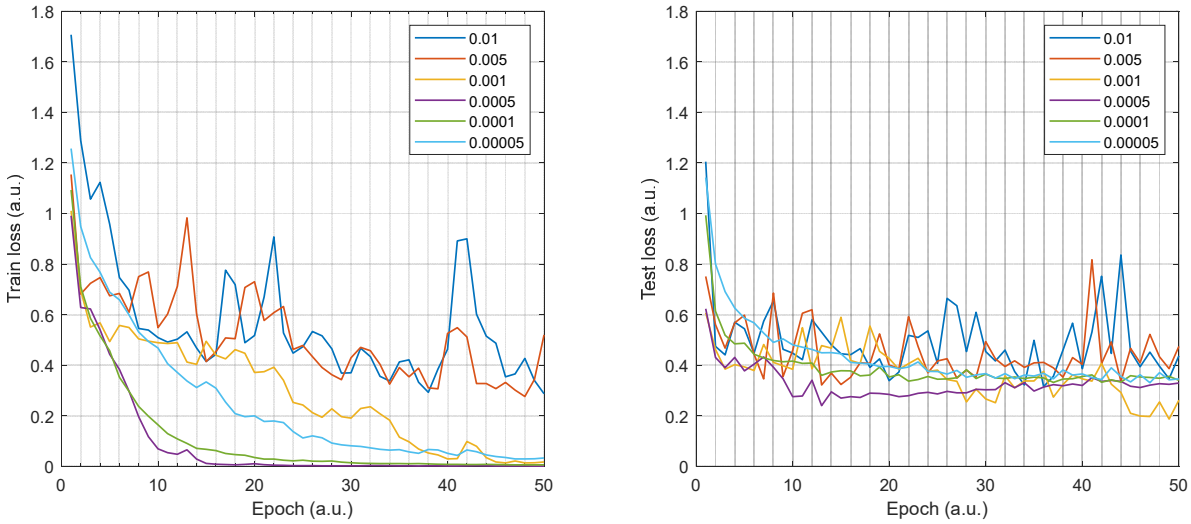

Figure 13. Loss values of the test set at different learning rates, each color represents a learning rate.

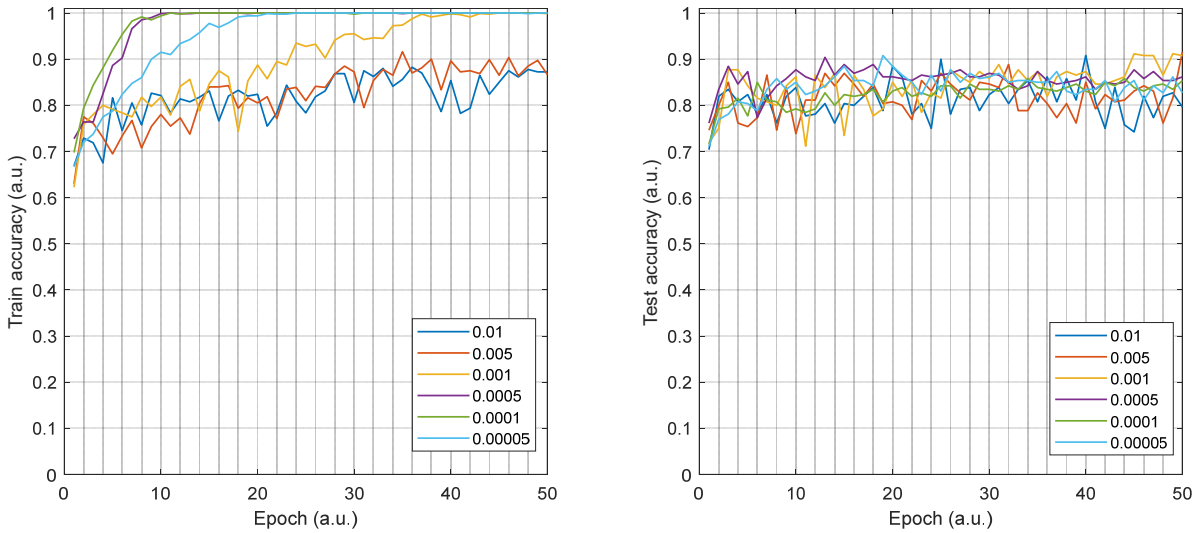

Figure 14. Accuracies of the training set and test set at different learning rates, each color represents a learning rate.

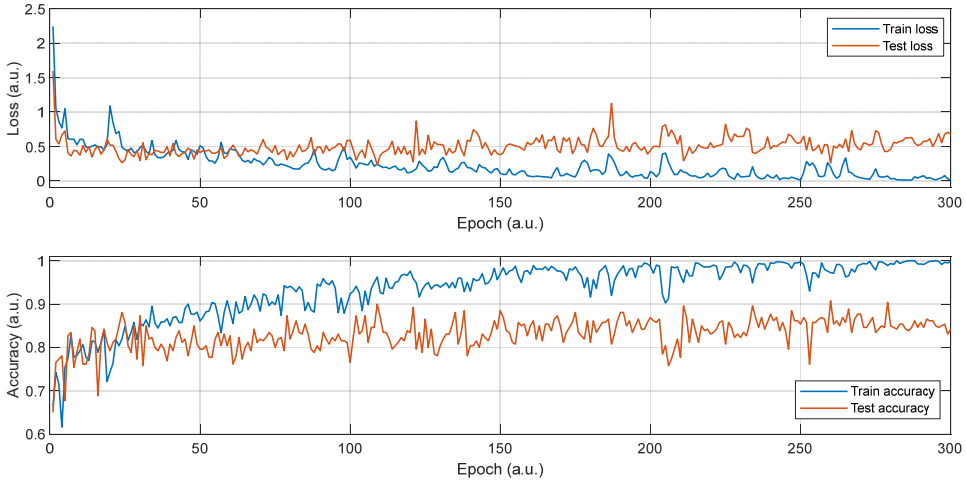

Figure 15. Loss values and accuracies when the learning rate was 0.01.

3.2. Discussion

(1) In this study, visible/near-infrared light was used to irradiate banana wilt leaves, due to the damage caused by the pathogen of banana Fusarium wilt disease to the vascular system of plant, the internal tissue structure and chemical composition of plant leaves underwent changes, the Fusarium wilt leaves selectively absorbed visible/near-infrared light of different wavelengths, and the reflected visible/infrared light carried information about the composition and structure of the wilt leaves, not just nutrient information. In this study, reflectance spectrum data were obtained through visible/near-infrared spectroscopy technology, and the spectral information was analyzed relating to the composition and structure of banana Fusarium wilt leaf using mathematical models, which can achieve the identification and severity grading of banana leaf Fusarium wilt disease.

(2) For the grading detection of the latent period and onset period of banana Fusarium wilt disease, when establishing a disease severity grading model using conventional machine learning methods, the grading effect of the model was related to the spectral data preprocessing method and modeling method. The FD preprocessing method not only improves the resolution of overlapping peaks, but also amplifies noise signals; therefore, the FD preprocessing method should be combined with preprocessing methods that can reduce spectral noise in order to improve the classification performance of the model. The goal of FDA is to find a linear projection that enables the best class separation of the projected data points in the new space, which can reduce the impact of noise on the model to some extent. ELM does not differentiate between effective signals and noise signals for classification modeling, so the classification performance of OD-FDA, FD-FDA, FD-SG-FDA, FD-MSC-FDA, and FD-MSC-SG-FDA models were better than those of OD-ELM, FD-ELM, FD-SG-ELM, FD-MSC-ELM, and FD-MSC-SG-ELM models correspondingly.

(3) When using 1D-CNN to establish the disease severity grading model for detecting the incubation period and onset period of banana Fusarium wilt disease, the grading effect of the model was related to the hyperparameters of the 1D-CNN model. In this study, the focus was on analyzing the impact of the learning rate on model performance. Both larger and smaller learning rates had a negative impact on the model's performance, and it was necessary to select the optimal learning rate. In this study, comparative analysis was conducted and found that when the learning rate was set to 0.0005, the grading model had the best classification performance. In the later stage, we would study the influence of other hyperparameters on the model performance and select the best combination of hyperparameters.

(4) Using conventional machine learning methods to establish a banana Fusarium wilt disease severity grading model required the preprocessing of the spectral data; meanwhile, using 1D-CNN to establish the disease severity grading model did not require the preprocessing of spectral data and could achieve the same model effect as using conventional

machine learning methods. Conventional machine learning models were suitable for single, stable environmental conditions, while 1D-CNN was suitable for more complex and variable environmental conditions, making the 1D-CNN model more practical. Subsequent research would establish a 2D-CNN grading model for the severity of banana Fusarium wilt disease based on visible/near-infrared spectral curve images.

4. Conclusions

In this study, visible/near-infrared spectroscopy was used to explore the feasibility of disease detection during banana Fusarium wilt latency and onset periods. A portable visible/near-infrared spectroscopy acquisition system was constructed, and a variety of disease classification models were established. By analyzing the disease detection results during banana Fusarium wilt latent and onset periods, the following conclusions were drawn:

(1) This research method could realize the detection of banana Fusarium wilt in the latent period and could realize the grading detection of the disease in the onset period.
(2) It was necessary to preprocess the spectral data when using conventional machine learning methods to establish the classification model for the severity of banana Fusarium wilt disease. The results showed that the MSC and SG smoothing preprocessing methods improved the classification effect of the banana Fusarium wilt disease grade classification model. Using 1D-CNN to establish the disease severity grading model did not require preprocessing of spectral data, the 1D-CNN modeling method was suitable for complex and changing environmental conditions and had stronger practicality than conventional machine learning methods.
(3) In this study, we explored the development of a rapid in vivo detection method for the disease grade of banana Fusarium wilt in the latent and onset periods, providing methods and data support for the effective control of banana Fusarium wilt.

Author Contributions: Conceptualization, C.L. (Cuiling Li); methodology, C.L. (Cuiling Li) and D.X.; software, C.L. (Cuiling Li); validation, C.L. (Cuiling Li); formal analysis, C.L. (Chunyu Li); investigation, D.X. and S.Y.; resources, X.W. and C.L. (Chunyu Li); data curation, S.Y.; writing—original draft preparation, C.L. (Cuiling Li); writing—review and editing, X.W. and C.L. (Chunyu Li); visualization, S.Y.; supervision, X.W. and C.L. (Chunyu Li); funding acquisition, S.Y. All authors have read and agreed to the published version of the manuscript.

Funding: This research was made possible by the following: (1) the National Key Research and Development Plan Project (2022YFD2001402); (2) the Outstanding Scientist Program of Beijing Academy of Agriculture and Forestry Sciences (JKZX202212); (3) the Reform and Development Project of Beijing Academy of Agriculture and Forestry Sciences-Asparagus mother stem blight inspection robot based on canopy multispectral imaging technology; and (4) the Laboratory Construction Project of 2024 National Engineering Research Center for Intelligent Equipment in Agriculture (PT2024-41).

Data Availability Statement: The data presented in this study are available upon request from the corresponding author.

Acknowledgments: We are very thankful to Yukang Li for operating the visible/near-infrared spectrum acquisition system in the banana plantation, Haowei Liu for taking take photos of the experiment site, Mingzhou Chen for the literature collection, and Changyuan Zhai for making enlightening suggestions in this study.

Conflicts of Interest: The authors declare no conflicts of interest.

References

1. Selvaraj, M.G.; Vergara, A.; Montenegro, F.; Alonso Ruiz, H.; Safari, N.; Raymaekers, D.; Ocimati, W.; Ntamwira, J.; Tits, L.; Omondi, A.B.; et al. Detection of banana plants and their major diseases through aerial images and machine learning methods: A case study in DR Congo and Republic of Benin. *ISPRS J. Photogramm. Remote Sens.* **2020**, *169*, 110–124. [CrossRef]
2. Olivares, B.O.; Rey, J.C.; Lobo, D.; Navas-Cortés, J.A.; Gómez, J.A.; Landa, B.B. Fusarium wilt of bananas: A review of agroenvironmental factors in the Venezuelan production system affecting its development. *Agronomy* **2021**, *11*, 986. [CrossRef]

3. Ploetz, R.C. Management of Fusarium wilt of banana: A review with special reference to tropical race 4. *Crop Prot.* **2015**, *73*, 7–15. [CrossRef]
4. Blomme, G.; Dita, M.; Jacobsen, K.S.; Vicente, L.P.; Molina, A.; Ocimati, W.; Poussier, S.; Prior, P. Bacterial diseases of bananas and enset: Current state of knowledge and integrated approaches toward sustainable management. *Front. Plant Sci.* **2017**, *8*, 1290. [CrossRef] [PubMed]
5. Nakkeeran, S.; Rajamanickam, S.; Saravanan, R.; Vanthana, M.; Soorianathasundaram, K. Bacterial endophytome-mediated resistance in banana for the management of *Fusarium* wilt. *3 Biotech* **2021**, *11*, 267. [CrossRef]
6. Ordonez, N.; Seidl, M.F.; Waalwijk, C.; Drenth, A.; Kilian, A.; Thomma, B.P.H.J.; Ploetz, R.C.; Kema, G.H.J.; Sheppard, D.C. Worse comes to worst: Bananas and Panama disease-when plant and pathogen clones meet. *PLoS Pathog.* **2015**, *11*, e1005197. [CrossRef]
7. Lin, Y.H.; Lin, Y.J.; Chang, T.D.; Hong, L.L.; Chen, T.Y.; Chang, P.F.L. Development of a TaqMan probebased insulated isothermal polymerase chain reaction (iiPCR) assay for detection of *Fusarium oxysporum* f. sp. *cubense* race 4. *PLoS ONE* **2016**, *11*, e0159681.
8. Shen, Z.; Xue, C.; Penton, C.R.; Thomashow, L.S.; Zhang, N.; Wang, B.; Ruan, Y.; Li, R.; Shen, Q. Suppression of banana Panama disease induced by soil microbiome reconstruction through an integrated agricultural strategy. *Soil Biol. Biochem.* **2019**, *128*, 164–174. [CrossRef]
9. Dita, M.A.; Waalwijk, C.; Buddenhagen, I.W.; Souza, M.T., Jr.; Kema, G.H.J. A molecular diagnostic for tropical race 4 of the banana fusarium wilt pathogen. *Plant Pathol.* **2010**, *59*, 348–357. [CrossRef]
10. Siamak, S.B.; Zheng, S.J. Banana fusarium wilt (*Fusarium oxysporum* f. sp. *cubense*) control and resistance, in the context of developing wilt-resistant bananas within sustainable production systems. *Hortic. Plant J.* **2018**, *4*, 208–218. [CrossRef]
11. Li, H.; Li, Y.; Nie, Y. Research status of occurrence and control of Fusarium wilt of banana. *J. South China Agric. Univ.* **2019**, *40*, 128–136.
12. Zhang, S.; Li, X.; Ba, Y.; Lyu, X.; Zhang, M.; Li, M. Banana Fusarium Wilt Disease Detection by Supervised and Unsupervised Methods from UAV-Based Multispectral Imagery. *Remote Sens.* **2022**, *14*, 1231. [CrossRef]
13. Lin, Y.J.; Lin, H.K.; Lin, Y.H. Construction of Raman spectroscopic fingerprints for the detection of Fusarium wilt of banana in Taiwan. *PLoS ONE* **2020**, *15*, e0230330. [CrossRef] [PubMed]
14. Lin, Y.H.; Chang, J.Y.; Liu, E.T.; Chao, C.P.; Huang, J.W.; Chang, P.F.L. Development of a molecular marker for specific detection of *Fusarium oxysporum* f. sp. *cubense* race 4. *Eur. J. Plant Pathol.* **2009**, *123*, 353–365. [CrossRef]
15. Fraser-Smith, S.; Czislowski, E.; Meldrum, R.A.; Zander, M.; O'Neill, W.; Balali, G.R.; Aitken, E.A.B. Sequence variation in the putative effector gene SIX8 facilitates molecular differentiation of *Fusarium oxysporum* f. sp. *cubense*. *Plant Pathol.* **2014**, *63*, 1044–1052. [CrossRef]
16. Yang, L.L.; Sun, L.X.; Ruan, X.L.; Qiu, D.Y.; Chen, D.H.; Cai, X.Q.; Li, H.P. Development of a single-tube duplex realtime fluorescence method for the rapid quantitative detection of *Fusarium oxysporum* f. sp. *Cubense* race 1 (FOC1) and race 4 (FOC4) using TaqMan probes. *Crop Prot.* **2015**, *68*, 27–35. [CrossRef]
17. Li, B.; Du, J.; Lan, C.; Liu, P.; Weng, Q.; Chen, Q. Development of a loop-mediated isothermal amplification assay for rapid and sensitive detection of *Fusarium oxysporum* f. sp. *cubense* race 4. *Eur. J. Plant Pathol.* **2013**, *135*, 903–911. [CrossRef]
18. Peng, J.; Zhang, H.; Chen, F.; Zhang, X.; Xie, Y.; Hou, X.; Li, G.; Pu, J. Rapid and quantitative detection of *Fusarium oxysporum* f. sp. *cubense* race 4 in soil by real-time fluorescence loop-mediated isothermal amplification. *J. Appl. Microbiol.* **2014**, *117*, 1740–1749. [CrossRef]
19. Zhang, X.; Zhang, H.; Pu, J.; Qi, Y.; Yu, Q.; Xie, Y.; Li, G.; Pu, J. Development of a real-time fluorescence loop-mediated isothermal amplification assay for rapid and quantitative detection of *Fusarium oxysporum* f. sp. *cubense* tropical race 4 in soil. *PLoS ONE* **2013**, *8*, e82841. [CrossRef]
20. Schaad, N.W.; Frederick, R.D.; Shaw, J.; Schneider, W.L.; Hickson, R.; Petrillo, M.D.; Luster, D.G. Advances in molecular-based diagnostics in meeting crop biosecurity and phytosanitary issues. *Annu. Rev. Phytopathol.* **2003**, *41*, 305–324. [CrossRef]
21. Deng, L.; Mao, Z.; Li, X.; Hu, Z.; Yan, Y. UAV-based multispectral remote sensing for precision agriculture: A comparison between different cameras. *ISPRS J. Photogramm.* **2018**, *146*, 124–136. [CrossRef]
22. Nakato, G.V.; Beed, F.; Bouwmeester, H.; Ramathani, I.; Mpiira, S.; Kubiriba, J.; Nanavati, S. Building agricultural networks of farmers and scientists via mobile phones: Case study of banana disease surveillance in Uganda. *Can. J. Plant Pathol.* **2016**, *38*, 307–316. [CrossRef]
23. Ye, H.; Huang, W.; Huang, S.; Cui, B.; Dong, Y.; Guo, A.; Ren, Y.; Jin, J. Identification of banana fusarium wilt using supervised classification algorithms with UAV-based multi-spectral imagery. *Int. J. Agric. Biol. Eng.* **2020**, *13*, 136–142. [CrossRef]
24. Khodabakhshian, R.; Abbaspour-Fard, M.H. Pattern recognition-based spectroscopyfor non-destructive detection of pomegranates during maturity. *Spectrochim. Acta Part A Mol. Biomol. Spectrosc.* **2020**, *231*, 118127. [CrossRef] [PubMed]
25. Zhu, W.; Cheng, F. Analysis of Transgenic and Non-Transgenic Rice Leaves Using Visible/Near-Infrared Spectroscopy. *Spectrosc. Spectr. Anal.* **2012**, *32*, 4.
26. Ren, D.; Shen, J.; Ren, S.; Wang, J.; Lu, A. An X-Ray Fluorescence Spectroscopy Pretreatment Method for Detection of Heavy Metal Content in Soil. *Spectrosc. Spectr. Anal.* **2018**, *38*, 3934–3940.
27. Liu, P.; Wang, J.; Li, Q.; Gao, J.; Tan, X.Y.; Bian, X.H. Rapid identification and quantification of *Panax notoginseng* with its adulterants by near infrared spectroscopy combined with chemometrics. *Spectrochim. Acta A Mol. Biomol. Spectrosc.* **2019**, *206*, 23–30. [CrossRef]

28. Bian, X.H.; Chen, D.; Cai, W.S.; Grant, E.R.; Shao, X.G. Rapid determination of metabolites in bio-fluid samples by Raman spectroscopy and optimum combinations of chemometric methods. *Chin. J. Chem.* **2011**, *29*, 2525–2532. [CrossRef]
29. Yahya, K.A.; Samsuzana, A.A.; Siti, K.B.; Nazmi, M.N.; Idris, A.S.; Anuar, I.M. Development of classification models for basal stem rot (BSR) disease in oil palm using dielectric spectroscopy. *Ind. Crops Prod.* **2018**, *124*, 99–107.
30. Abdulridha, J.; Ampatzidis, Y.; Ehsani, R.; de Castro, A.I. Evaluating the performance of spectral features and multivariate analysis tools to detect laurel wilt disease and nutritional deficiency in avocado. *Comput. Electron. Agric.* **2018**, *155*, 203–211. [CrossRef]
31. Siedliska, A.; Baranowski, P.; Zubik, M.; Mazurek, W.; Sosnowska, B. Detection of fungal infections in strawberry fruit by VNIR/SWIR hyperspectral imaging. *Postharvest Biol. Technol.* **2018**, *139*, 115–126. [CrossRef]
32. Liu, T.; Xu, T.; Yu, F.; Yuan, Q.; Guo, Z.; Xu, B. A method combining ELM and PLSR (ELM-P) for estimating chlorophyll content in rice with feature bands extracted by an improved ant colony optimization algorithm. *Comput. Electron. Agric.* **2021**, *186*, 106177. [CrossRef]
33. *NY/T 2248-2012*; Evaluation Technical Code of Tropical Crop Germplasm for Resistance to Pests—Banana Sigatoka, Banana Fusarium wilt and Banana Root Knot Nematode Disease. Agricultural Industry Standards of the People's Republic of China: Beijing, China, 2012.
34. Zhang, J.; Liu, P.; Che, H.; Zhang, X.; Yuan, L.; Wu, K.; Zhou, X.; Zhang, Y. A Near-Earth Hyperspectral Data Extension Method Applied to Deep Learning. China Patent CN110070004A, 26 August 2024.
35. Jolliffe, I.T.; Cadima, J. Principal component analysis: A review and recent developments. *Philos. Trans. R. Soc. A Math. Phys. Eng. Sci.* **2016**, *374*, 20150202. [CrossRef] [PubMed]
36. Jahirul, M.I.; Rasul, M.G.; Brown, R.J.; Senadeera, W.; Mahlia, T.M.I. Investigation of correlation between chemical composition and properties of biodiesel using principal component analysis (PCA) and artificial neural network (ANN). *Renew. Energy* **2021**, *168*, 632–646. [CrossRef]
37. Huang, G.B.; Zhu, Q.Y.; Siew, C.K. Extreme learning machine: Theory and applications. *Neurocomputing* **2006**, *70*, 489–501. [CrossRef]
38. Adnan, R.M.; Liang, Z.; Trajkovic, S.; Zounemat-Kermani, M.; Kisi, O. Daily streamflow prediction using optimally pruned extreme learning machine. *J. Hydrol.* **2019**, *577*, 123981. [CrossRef]
39. Pu, S.; Zheng, E.; Chen, B. Research on A Classification Algorithm of Near-Infrared Spectroscopy Based on 1D-CNN. *Spectrosc. Spectr. Anal.* **2023**, *43*, 2446–2451.
40. Tang, J.; Luo, Y.; Li, X.; Chen, Y.; Wang, P.; Lu, T.; Ji, X.; Pang, Y.; Zhu, L. Study on One-Dimensional Convolutional Neural Network Model Based on Near-Infrared Spectroscopy Data. *Spectrosc. Spectr. Anal.* **2024**, *44*, 731–736.
41. Zhang, D.; Zhang, J.; Peng, B.; Wu, T.; Jiao, Z.; Lu, Y.; Li, G.; Fan, X.; Shen, S.; Gu, A.; et al. Hyperspectral model based on genetic algorithm and SA-1DCNN for predicting Chinese cabbage chlorophyll content. *Sci. Hortic.* **2023**, *321*, 112334. [CrossRef]